



Effect of Test Temperature and Strain Rate on Dynamic Mechanical Behavior of Aluminum Alloy 2519A

Ling-ying Ye, Yu Dong, Yong Zhang, Da-xiang Sun, and Xin-ming Zhang

(Submitted October 15, 2018; in revised form May 16, 2019; published online July 23, 2019)

The dynamic mechanical behavior of aluminum alloy 2519A-T9I6 has been investigated by a split Hopkinson bar at temperature range from 298 to 523 K and at strain rates of from 10^3 to $5 \times 10^3 \text{ s}^{-1}$ in this study. The results show that both the strain rate and test temperature have a significant effect on the dynamic behavior and microstructure evolution of aluminum alloy 2519A-T9I6. Under similar strain rate, the strengthening effect of strain rate decreases with the increase in the test temperature. Moreover, the dynamic yield strength at above 423 K drops sharply at the strain rate of about 5000 s^{-1} , which is attributed to the flow softening caused by decomposition of θ' precipitates at high strain rate and high temperature.

Keywords 2519A, decomposition of θ' precipitates, dynamic yield strength, high strain rate, split Hopkinson bar

1. Introduction

An age-hardenable aluminum alloy named 2519A alloy has been widely used in military applications. For some specific applications, such as ballistic armors, the dynamic mechanical properties should be concerned as the materials may experience rapid change in temperature and strain in a very short time (less than 100 μs) during the dynamic impact (Ref 1-3). Although constitutive equation of 2519A alloy involving test temperature and strain rate has been established, systematic observation of the evolution of microstructure during dynamic impacting still needs to be made. For the structure design of real ballistic applications, it is of great importance to characterize the effects of test temperature and strain rate on the dynamic behavior of 2519A alloy, as well as its microstructure evolution.

Although most structure materials demonstrate a different response when increasing test temperatures or strain rates, yet higher dynamic mechanical properties do associate with higher general mechanical properties. Gu and his co-workers have demonstrated that the strength of alloy 2519A can be further improved by interrupted aging process (Ref 4-6). The interrupted aging process named “T9I6” (solution treatment, quenching, pre-aging, pre-deformation, interrupted aging and reaging) could reduce the average size of the strengthening phase and increase its volume fraction in 2519A alloy, which is

beneficial to both its mechanical properties and dynamic impact resistance. According to Gu, the maximum tensile strength of 2519A alloy can reach 540.1 MPa, while the elongation can reach 14.3% (Ref 4). Actually, several works have been done to show that 2519A alloys with T9I6 temper performs well under dynamic impact at room temperature (Ref 5, 7), which can provide fundamental insight into the microstructure evolution and dynamic mechanical behavior with different test temperatures and strain rates.

Microstructure changes during the impact moment need to be clarified, and they can significantly influence ballistic performance. Thus, the microstructure in 2519A alloy will undergo a significant change under dynamic impact and it will lead to unexpected behavior. Perrin (Ref 8) pointed out that the metastable phase stable at room temperature will evolve at high strains and strain rates. Therefore, the metastable θ' phase (Al_2Cu) may coarsen and the dynamic impact resistance may deteriorate while impacting. Gao (Ref 9, 10) firstly studied the dynamic impact of 2519A alloy and found the extension of θ' phase into θ phase at high strain rate. To better understand the influences of temperature and strain rate on adiabatic shearing behavior, adiabatic shear bands (ASBs) were detected in the impacted 2519A alloy sample. Liu Ref 11 pointed out that dynamic yield strength of 2519A alloy decreases with the rise of the test temperature, and the dynamic recrystallization character can be observed in the alloy. In the last 5 years, Al-Cu-Mg alloy with high Cu-to-Mg ratio has been an important area of research (Ref 12-16). It has been proved that 2519A alloy is a promising engineering material for aircraft and automotive structural components (Ref 7, 17). However, previous researches pay little attention on dynamic impact property and microstructural evolution under elevated temperature and very few of them involve aluminum alloy under interrupted aging like T9I6.

The present work hereby designed a series of dynamic impact experiments under test temperature of 298, 423 and 523 K, at constant strain rates of 1040, 2400, 3500 and 5040 s^{-1} , involving the split Hopkinson pressure bar. The stress-strain relation of dynamic behavior and the evolution of the microstructure are discussed. The results will be helpful for the estimation of the dynamic impact resistance and application prospect for 2519A-T9I6 alloy.

Ling-ying Ye, Yu Dong, Yong Zhang, and Xin-ming Zhang, School of Materials Science and Engineering, Central South University, Changsha 410083, China; Da-xiang Sun, Guangdong Industry Analysis Testing Center, Guangzhou 510650, China. Contact e-mail: yong.zhang@csu.edu.cn.

2. Experimental Details

Aluminum alloy 2519A plate was commercially produced, and the chemical composition of aluminum alloy 2519A plate is given in Table 1.

The as-received plate was solutionized at 808 K for 2 h and followed by water quenching and artificial aging at 438 K for 2 h. Then the plate was rolled with a reduction rate of 15%. Finally, the plate was interrupted-aged at 338 K for 120 h and reaged at 338 K for 10 h. The entire heat treatment process is called T9I6 process. For dynamic impact experiment, the height of sample needs to be minimized to ensure reliable dynamic properties (Ref 9). In the experiment, the cylindrical specimens (4 mm height and 6 mm diameter) were cut along the normal direction (ND) of the 2519A rolling plate to show greater tendency to form transformed bands (Ref 15). Dynamic impact tests were performed using a compressive split Hopkinson pressure bar (SHPB) equipment where the cylindrical specimen is stroked by a high-velocity collision steel bar. The schematic of SHPB device has already been described (Ref 10). In the process of dynamic impact, the incident stress wave is generated instantaneously, which can only be recorded by the resistance strain gauge attached to the incident bar. At the same time, strain gauge attached to the transmission bar recorded the portion of wave that transmitted into the specimen. The electrical signal is then transmitted to the recording device. Since the friction by the specimen and the bars may affect the experimental results, grease was used on the contact surface before dynamic impact experiment. The setting impact strain rates are 1040, 2400, 3500 and 5040 s⁻¹. Due to different materials' behavior, the measured strain rates may vary slightly from the setting values. Temperature variations on the split Hopkinson bar were achieved by a hot air blower. The hot air blower continuously blows heated air to sample to make the sample reach the required temperature. The temperature of the sample is monitored by a chromel–alumel thermocouple attached directly to the sample. Before impacting, the samples for high-temperature tests were hold at 423 and 523 K for about 10 min. All the dynamic impact tests have been carried out at 298, 423 and 523 K, respectively, and the stress–strain curves were recorded.

The microstructure characterization was carried out using optical microscopy (OM) and transmission electron microscopy (TEM) along the cross section of specimens, as the samples were compressed to 1–2 mm thick. The TEM specimens were ground down to about 80 μm and cut into small disks (3 mm diameter), and then electropolished in an acid solution (80% methanol and 20% nitric acid) at about 243–253 K with a voltage of 20 V. And then the specimens were observed by a JEM-2100F analytical transmission electron microscope (TEM). The acceleration voltage is 200 kV.

Table 1 Composition of aluminum alloy 2519A (mass fraction, %)

Cu	Mg	Mn	Zr	Ti	Fe	Si	Al
5.80	0.20	0.30	0.20	0.05	0.15	0.04	Bal.

3. Results and Discussion

The recorded true stress–strain curves of alloy 2519A are shown in Fig. 1. The stress–strain curves of similar strain rate at different temperature conditions are shown in one single figure. It is demonstrated that the flow stress of the alloy decreases dramatically with the increase in the test temperatures for a given impact strain rate condition. That is to say, the increment in temperature weakens the strengthening effect of strain rate. Comparing all these curves in Fig. 1, it is found that, for higher strain rate and higher test temperature, the slope of curve becomes gentler before initial yielding. Moreover, when comparing different impact strain rate conditions, the alloy deformed more at high strain rate than low strain rate, as the stress–strain curves expanded further. The effect of test temperature is more pronounced on flow stress, while the effect of strain rate is more obvious on strain.

For the test temperature condition, the flow stress values increase with increasing strain rate. The first peak value in true stress–strain curve is defined as the dynamic yield strength (DYS), and the DHS values are marked by small circle on the curves in Fig. 1. Due to the extremely short dynamic impact time, it can be considered that kinetic energy was completely absorbed by the specimen. By integrating the true stress–strain curve in Fig. 1, the values of absorption energy per unit volume of specimen were calculated. The values of DHS and absorption energy per unit volume are shown in Fig. 2.

Figure 2(a) shows that, at 298 K, the DHS values increase linearly from 637.5 to 699.9 MPa with increasing impact strain rate, suggesting that the strengthening effect of strain rate increases. Flow softening appears at high strain rate, which can be noticed but not significant at room temperature. The trend of the curve is different at elevated temperatures. At 423 K, the DHS values increase deeply from 530.7 to 642.4 MPa when the impact strain rate increases from ~ 1000 to ~ 3500 s⁻¹. This DHS value drops quickly to 575.0 MPa when impact strain rate increases to ~ 5000 s⁻¹. At 523 K, the DHS values gradually increase at the impact strain rate range of ~ 1000 to ~ 3500 s⁻¹, demonstrating a descent trends at impact strain rate range of ~ 3500 s⁻¹ and above. The decrease in DHS at ~ 5000 s⁻¹ indicates that temperature is the key role in flow softening.

The integrated values here illustrate the absorption energy that has been disputed by the deformation of materials during whole impact process (Ref 18). The calculated values are shown in Fig. 2(b). It is demonstrated that the absorption energy increases linearly with increasing impact strain rate. It requires higher absorption energy at lower test temperature than at higher test temperature, and this trend is clearer at high impact strain rate ranges.

The temperature of sample after impact could raise significantly due to the energy absorption. According to Yi, the raised temperature can be estimated by the following equation (Ref 19):

$$T = T_0 + \frac{\beta}{\rho C_v} \int \sigma d\varepsilon \quad (\text{Eq 1})$$

where T is the adiabatic temperature, T_0 is the test temperature (which can be 298, 423 or 523 K in this research), β is an inverting factor (0.9), ρ is the density of 2519A alloy ($2.82 \times 10^3 \text{ kg m}^{-3}$), C_v is specific heat of 2519A alloy ($902 \text{ J kg}^{-1} \text{ K}^{-1}$), and σ and ε are true stress and true strain during whole impact process. The adiabatic temperatures of the

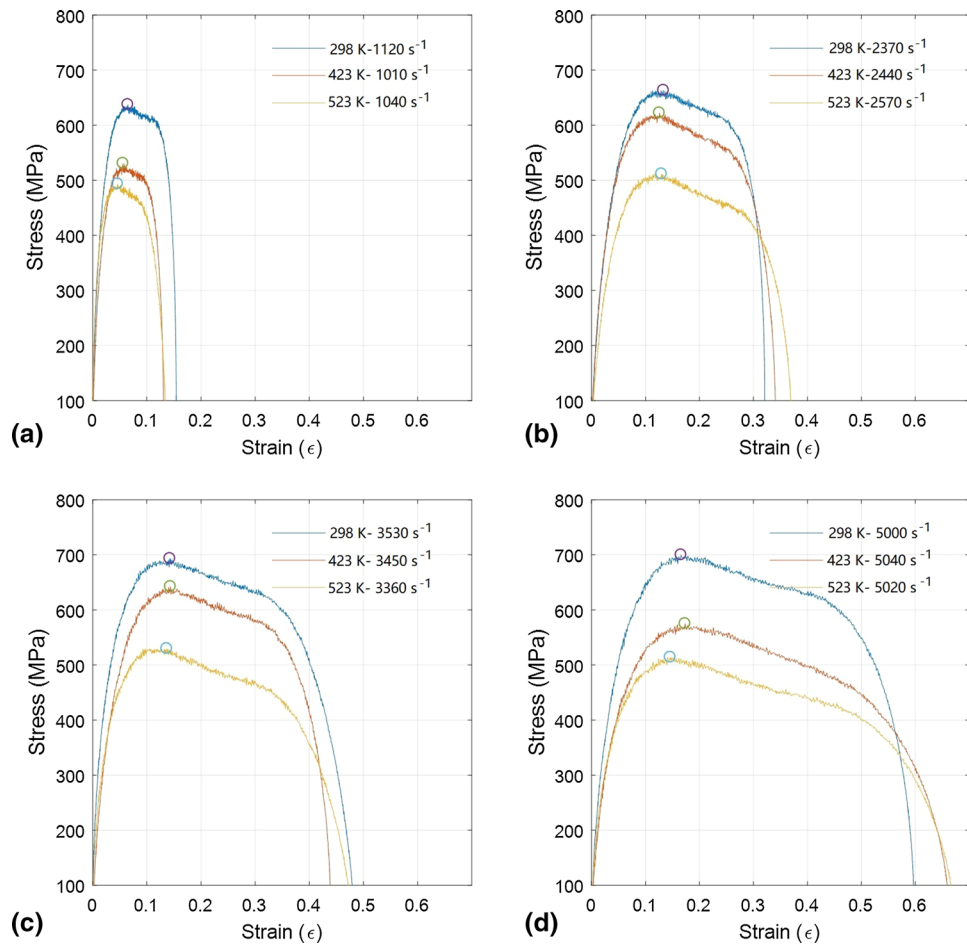


Fig. 1 True stress–strain relations of 2519A-T9I6 impacted at 298, 423 and 523 K under the strain rate of about: (a) 1000 s^{-1} , (b) 2400 s^{-1} , (c) 3500 s^{-1} and (d) 5000 s^{-1}

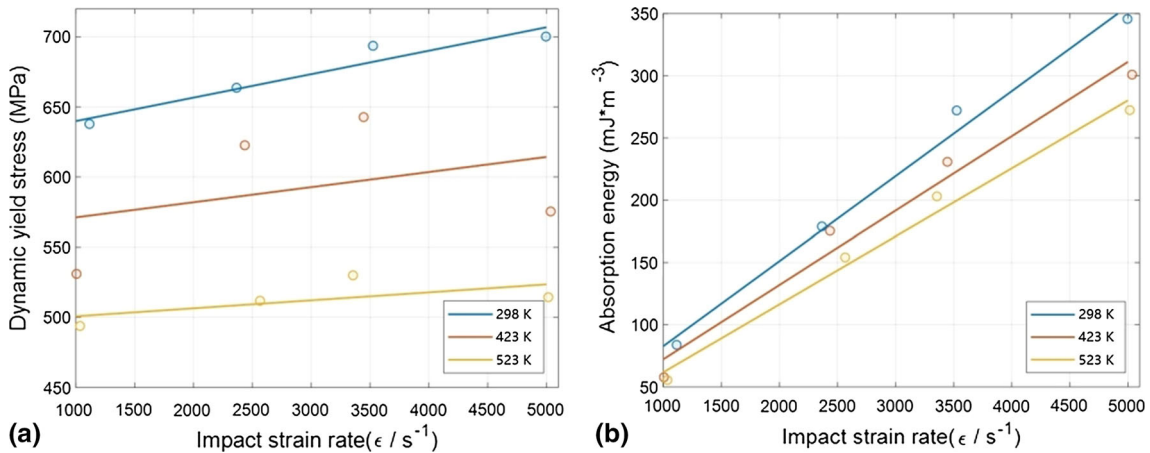


Fig. 2 (a) DYS values and (b) different absorption energies of samples at different impact strain rates

specimens impacted at 298, 423 and 523 K are calculated by Eq 1, and the results are shown in Fig. 3.

The experimental results show that at any temperature, the adiabatic temperature is positively correlated with the strain rate, and the magnitude of adiabatic temperature growth under three test temperature is very close. At the strain rate of about

1000 s^{-1} , the adiabatic temperature values of the samples impacted at 298, 423 and 523 K are about 322, 443 and 543 K, respectively. The value-added are 24, 20 and 20 K, respectively. When the strain rate reaches about 5000 s^{-1} , the values of adiabatic temperature are about 415, 529 and 620 K, and the value-added are 117, 106 and 97 K, respectively. Adiabatic

temperature has greater potential under room temperature test, and the temperature growth during adiabatic process gradually decreases with the increase in test temperature.

The flow softening at high strain rate is mainly caused by the thermal softening due to test temperature rise and adiabatic temperature rise. To observe the cross section of impact specimen is one of the effective methods to judge the mechanism of the dynamic yield strength decrease. When the alloy is impacted at 423 K and at strain rate of about 5000 s^{-1} , the dynamic yield strength declines sharply. The cross section of this specimen can be detected by means of metallographic observation, and the result is shown in Fig. 4. Adiabatic shear bands (ASBs) can be observed at 45° to the end surface of the specimen, and a few cracks can also be observed which means the failure has happened in the specimen. Local deformation is much larger than the average deformation through the whole sample, which means that the adiabatic temperature in ASBs is higher than the value calculated by Eq 1. ASBs are the main area that thermal softening happens. Similar ASBs can also be observed in sample impacted at 523 K and strain rate of about 5000 s^{-1} .

TEM bright-field images and corresponding selected area diffraction patterns (SADP) of 2519A-T9I6 impacted by different strain rates at 298, 423 and 523 K are shown in Fig. 5, 6 and 7, respectively. Al-Cu-Mg alloy is age-hardenable alloy. The 2519A aluminum alloy with high copper-to-magne-

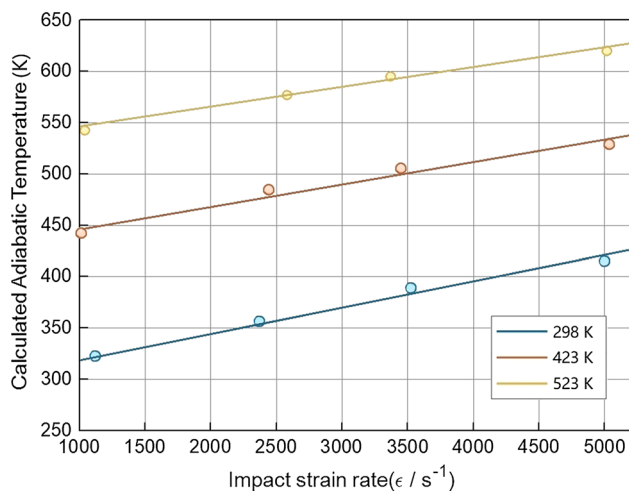


Fig. 3 Adiabatic temperature of aluminum alloy 2519A-T9I6 at different temperatures as a function of the strain rate

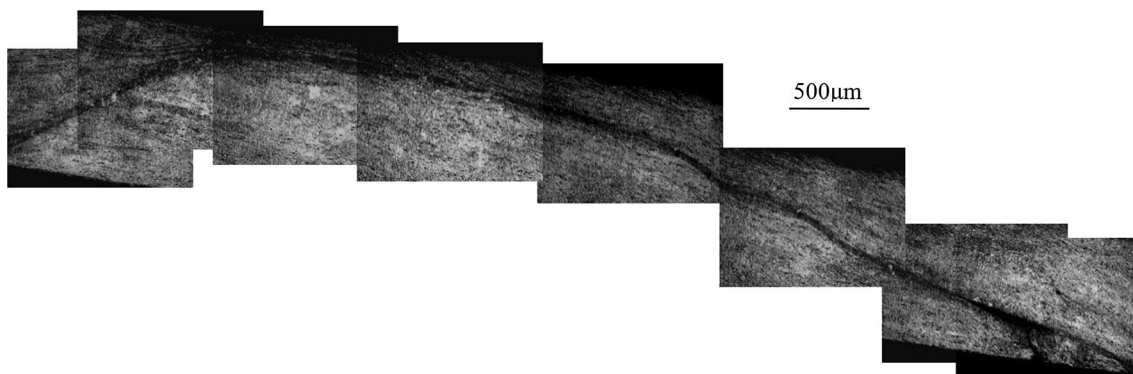


Fig. 4 Adiabatic shear bands of 2519A-T9I6 impacted at 423 K and strain rate of 5000 s^{-1}

sium ratio is mainly strengthened by θ' precipitates. The platelike θ' precipitate is semi-coherent with the Al matrix and its habit plan is $\{100\}_{\text{Al}}$ (Ref 20, 21) (Fig. 5a). When the test temperature is 298 K, only θ' precipitates are observed in the Al matrix from images and SADPs in Fig. 5(b) and (c). The orientation relationship between the θ' precipitates and the Al matrix is the same with specimen before impact. The density of θ' precipitates decreases significantly with the increase in strain rate. Moreover, SADP in Fig. 5(d) shows that there is no evolution of θ' precipitate into θ precipitate, even if the strain rate is up to 5000 s^{-1} .

For the specimens impacted at 423 K, when the strain rate is 1120 s^{-1} , some of the θ' precipitates are distorted, and some dislocations are observed in the specimen (Fig. 6a). When the strain rate reaches 3530 s^{-1} , the volume fraction of θ' precipitates decreases significantly and some spherical particles appear (Fig. 6b). It is detected that some θ' precipitates decompose and redissolve into the matrix, while the rest of θ' precipitates still exist in the matrix. At the strain rate of 5040 s^{-1} , almost all θ' precipitates are broken down and the extant precipitates in the matrix are all spherical (Fig. 6c), which can explain the decrease in the dynamic yield strength.

For the alloy impacted at 523 K and at strain rate of 1040 s^{-1} , θ' precipitates become finer, and some spherical precipitate appearance can be observed in the sample. But SADP shows that there are only θ' precipitates in the alloy (Fig. 7a). At the strain rate of 3370 s^{-1} , the volume fraction of θ' precipitates decreases significantly, which is the same thing as room temperature (Fig. 7b). However, the remaining θ' precipitates stay the same orientation relationship between Al matrix right now. When the strain rate reaches 5020 s^{-1} , the morphology and orientation of θ' precipitates are destroyed (Fig. 7c). The spherical phases arise from the coarsening of θ' precipitates. Diffraction spots that reflect precipitate in the SADP become arc, which means the rotation of θ' precipitates due to the happening of severe deformation. Therefore, it is indicated that the precipitates have poor stability at high temperature and high strain rate.

HRTEM micrographs of specimens impacting at 423 and 523 K corresponding to the strain rate of about 5000 s^{-1} are shown in Fig. 8. When the alloy impacted at 423 K, the precipitate is obviously distorted and there is the trace of dislocation cutting at the edge of the precipitate. And when the alloy impacted at 523 K, the precipitates are decomposed into different shapes. Moreover, whether the rod-shaped precipitate or the spherical, it can keep completely coherent boundary with Al matrix. The rod-shaped precipitate is discovered to have

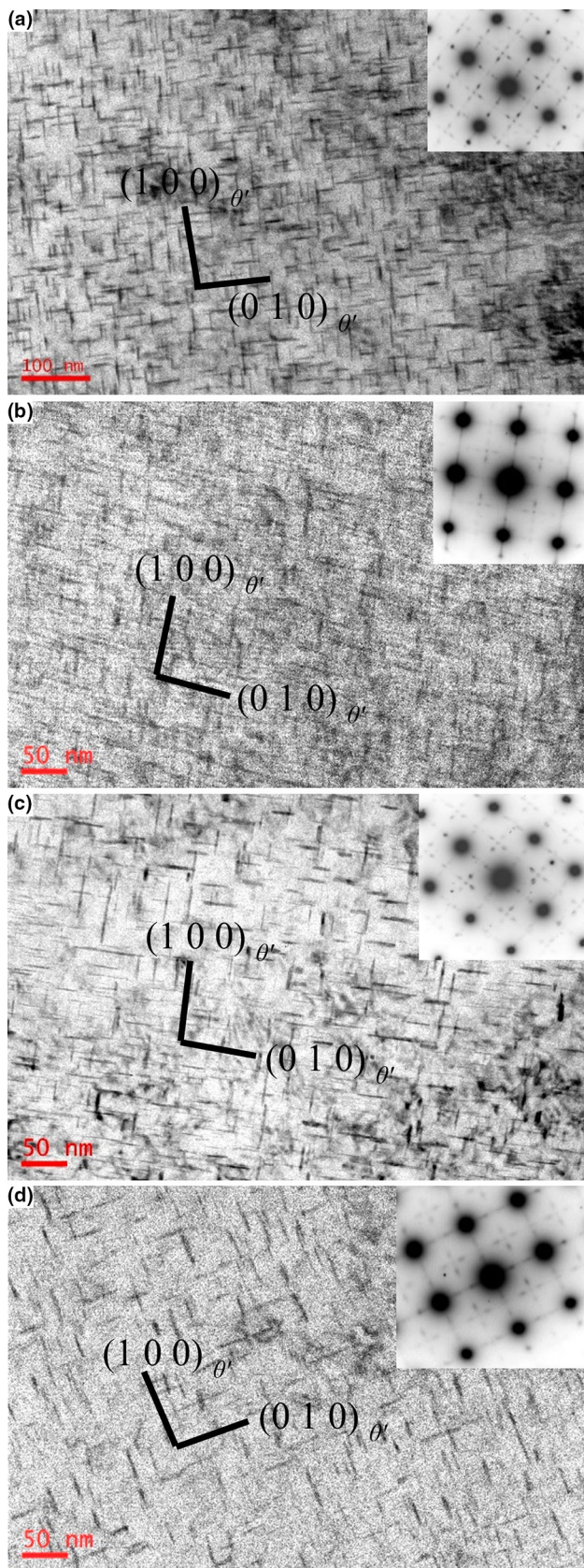


Fig. 5 TEM bright-field images and corresponding SADPs of 2519A-T916 impacted at different strain rates of: (a) before deformation, (b) 1120 s^{-1} , (c) 3530 s^{-1} and (d) 5000 s^{-1} at 298 K (the line indicates the $[100]_{\text{Al}}$ habit plane)

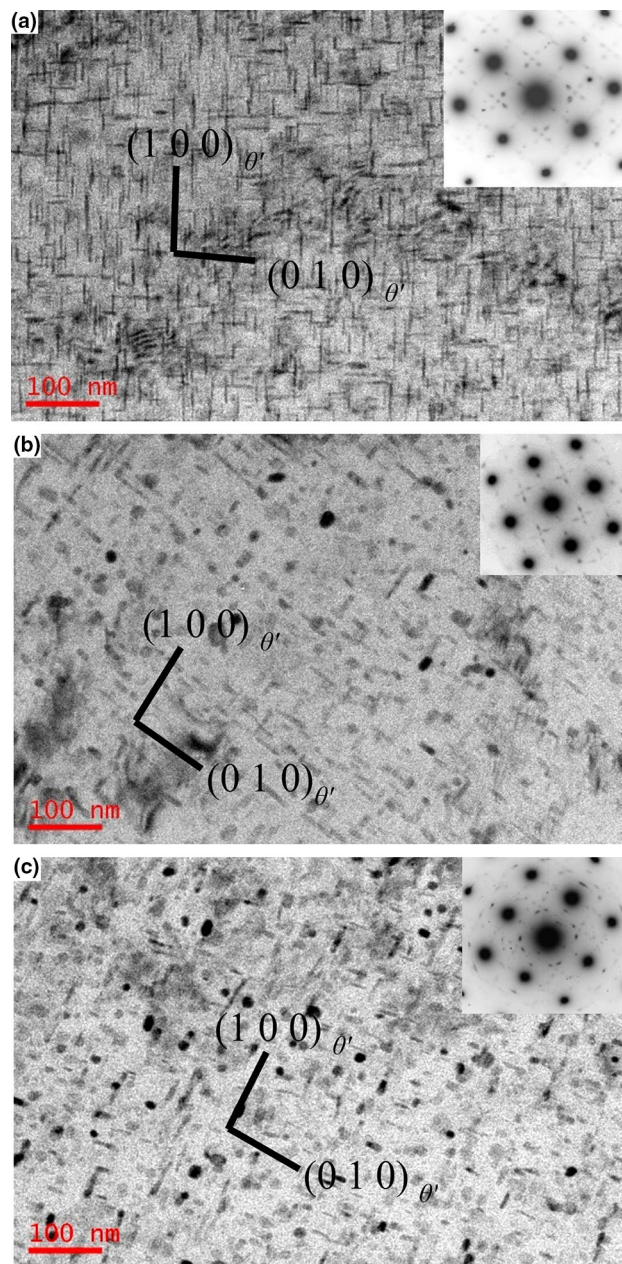


Fig. 6 TEM bright-field images and corresponding SADPs of 2519A-T916 impacted at different strain rates of: (a) 1110 s^{-1} , (b) 3450 s^{-1} and (c) 5040 s^{-1} at 423 K (the line indicates the $[100]_{\text{Al}}$ habit plane)

obvious signs of being cut at the edge, and there is no trace of incoherent θ phase appearance in the specimen. It is indicated that the evolution of θ' precipitate during dynamic impact at 523 K is mainly decomposition of θ' precipitate due to dislocation cutting.

Previous work (Ref 7) indicated dynamic impact at room temperature may bring a large amount of dislocations to 2519A alloy, and therefore, θ' precipitates are cut through and decomposed by dislocation. The dissociated precipitates will redissolve into Al matrix. The diffusion rate of solute atoms in dislocation is much higher than in Al matrix (Ref 21). Therefore, the diffusion of solute atoms under dynamic impact is much faster than under static process. According to the

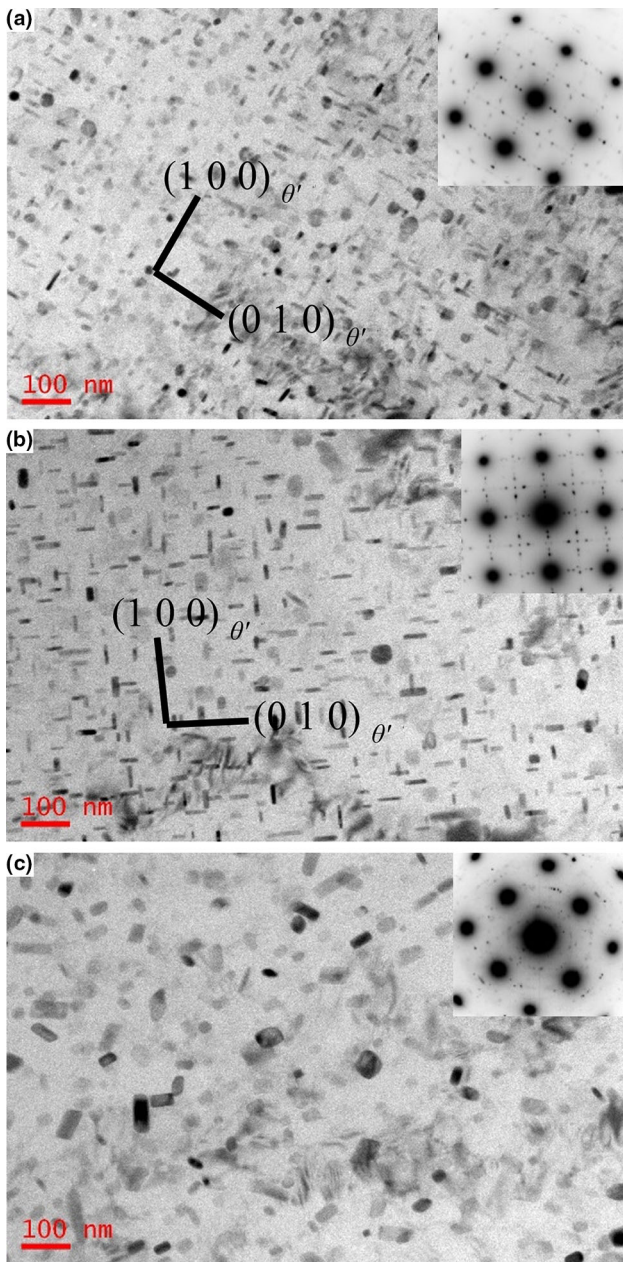


Fig. 7 TEM bright-field images and corresponding SADPs of 2519A-T916 impacted at different strain rates of: (a) 1040 s^{-1} , (b) 3370 s^{-1} and (c) 5020 s^{-1} at 523 K (the line indicates the $[100]\text{Al}$ habit plane)

empirical formula Eq 2, the dynamic diffusion coefficient is directly proportional to the plastic strain rate (Ref 22-24):

$$\frac{D'}{D_L} = 1 + \beta \dot{\epsilon} \quad (\text{Eq 2})$$

where D' is dynamic diffusion coefficient, D_L is static diffusion coefficient, $\dot{\epsilon}$ is strain rate, and β is coefficient of strain and strain rate. Due to Eq 2, diffusion coefficient could increase dramatically and the diffusion rate of solute atom is greatly improved during dynamic impact. Thus, there is significant increment in strain and strain rate in the dynamic impact. Therefore, θ' precipitates decompose in a very short period of time.

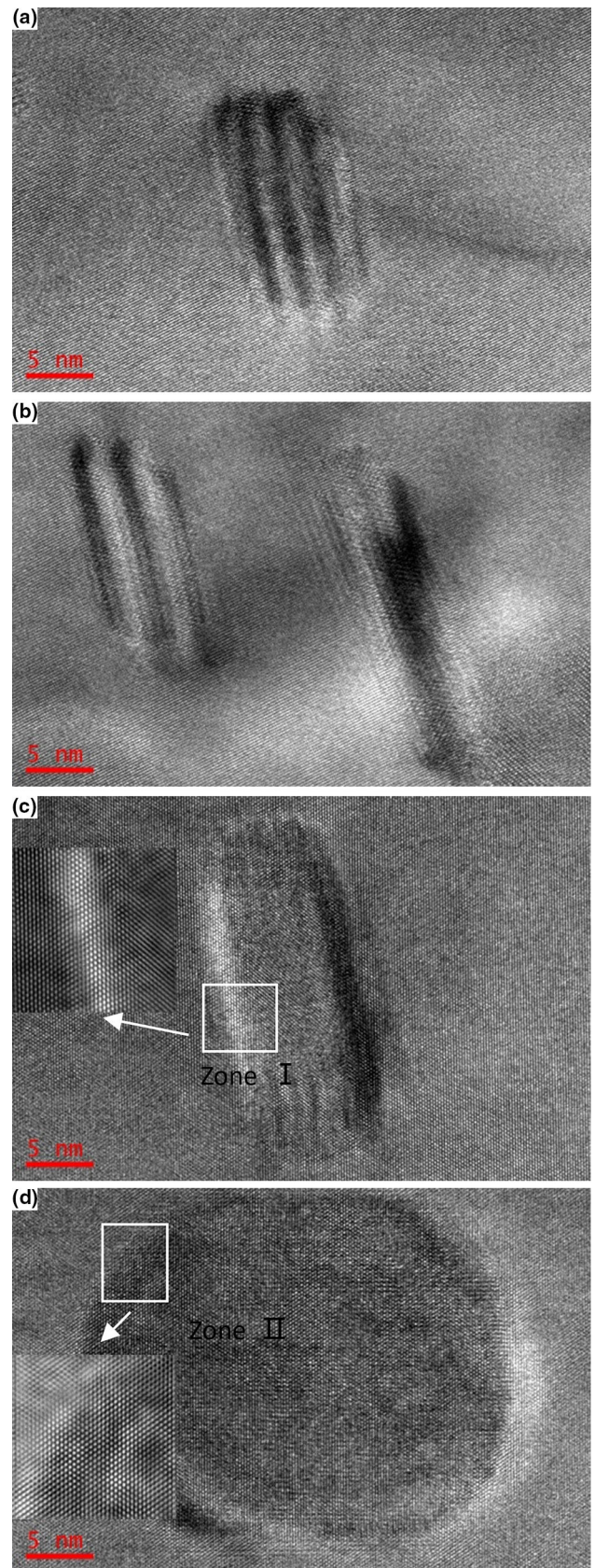


Fig. 8 HRTEM and FFT micrograph of precipitates in the 2519A-T916 specimen impacted at 423 and 523 K corresponding to the strain rate of about 5000 s^{-1} : (a), (b) 423 K and (c), (d) 523 K

At the same time, high temperature can also improve the diffusion rate of solute atoms. Therefore, the diffusion of solute atoms is much faster during dynamic impact at high temperature, which results in rapid decomposition of the precipitate and redissolution into Al matrix. In addition, it is considered that the whole process of dynamic impact would take about less than 100 μs , a quite short period of time. In such a short time, it is not enough for phase transformation from metastable θ' phase to stable θ phase. The width of θ' phase is thickened, which is due to atom diffusion from precipitate to Al matrix. Therefore, the decomposition of θ' precipitate is more likely to happen at high strain rate and high temperature.

Normally, it is equal opportunity for all variants of the precipitates' habit planes. In aged Al-Cu alloys, the platelike θ'' or θ' precipitates distribute over all three $\{100\}$ -plane variants in Al matrix and there is no obvious preferred orientation. Modified Orowan equations considering a strengthening stress provided by $\{100\}$ -plates have been developed and shown as follows (Ref 25):

$$\tau_p = 0.13G \frac{b}{(D_p t_p)^{1/2}} \left[f_v^{1/2} + 0.75(D_p/t_p)^{1/2} f_v + 0.14(D_p/t_p) f_v^{2/3} \right] \ln \frac{0.87(D_p t_p)^{1/2}}{r_0} \quad (\text{Eq 3})$$

where G is the shear modulus, b the magnitude of the Burgers vector, r_0 the interaction inner cutoff radius of the dislocation, f_v is the volume fraction, D_p the mean diameter and t_p the mean thickness of the precipitates. According to Eq 3, the yield strength is affected by the volume fraction, length and thickness of the precipitates. When the test temperature rises, the volume fraction of the precipitates decreases and some precipitates are thickened (Fig. 6 and 7), which makes τ_p values lower. Therefore, in addition to the temperature rise, the dynamic yield strength decreases mainly by the decomposition of θ' precipitates and redissolution into the Al matrix at high strain rate.

Interrupted aging "T9I6" process makes θ' precipitate finer and denser in 2519A alloy, which greatly improved the strength of the alloy. But during the high-velocity impact, finer precipitates are more likely to decompose by dislocation cutting. Therefore, the dynamic response of 2519A-T9I6 alloy is found to be very poor above strain rate of 5000 s^{-1} and at high temperature. For 2519A alloy, in order to improve the stability at elevated temperature, the size of θ' precipitates needs to be increased properly. But with the increase in the strengthening precipitates, the mechanical properties of the alloy are decreased, and how to solve this problem remains to be further studied in the future.

4. Conclusion

Dynamic impact experiments on 2519A-T9I6 have been carried out to investigate the effect of strain rate and test temperature on the dynamic mechanical properties and microstructure evolution. Both the strain rate and test temperature have significant effects on the compressive stress-strain response. Under similar strain rate, the dynamic yield strength decreases with the increase in the test temperature. Moreover, the values of dynamic yield strength at 423 and 523 K decline

sharply under the strain rate of about 5000 s^{-1} . Microstructure observations reveal the decomposition and redissolution of θ' precipitates during high-strain-rate and high-test-temperature deformation, which could result in the poor stability and low dynamic yield strength for 2519A alloy.

Acknowledgment

This study was supported by the National Key Research and Development Program of China (No. 2016YFB0300901), which is gratefully acknowledged.

References

1. E.A. Starke, Jr, and J.T. Staley, Application of Modern Aluminum Alloys to Aircraft, *Prog. Aerosp. Sci.*, 1996, **32**(2), p 131–172
2. J.J. Fisher, Jr., L.S. Kramer, and J.R. Pickens, Aluminum Alloy 2519 in Military Vehicles, *Adv. Mater. Processes*, 2002, **160**(9), p 43–46
3. L.S. Kramer, T.P. Blair, S.D. Blough, J.J. Fisher, Jr., and J.R. Pickens, Stress-corrosion Cracking Susceptibility of Various Product Forms of Aluminum Alloy 2519, *J. Mater. Eng. Perform.*, 2002, **11**(6), p 645–650
4. G. Gu, L.Y. Ye, X.M. Zhang, H.C. Jiang, D.X. Sun, and P. Zhang, Effects of Interrupted Ageing on Microstructure and Mechanical Properties of 2519A Aluminum Alloy, *Chin. J. Nonferr. Met.*, 2013, **23**(8), p 2098–2103
5. L.Y. Ye, G. Gu, X.M. Zhang, D.X. Sun, H.C. Jiang, and P. Zhang, Dynamic Properties Evaluation of 2519A Aluminum Alloy Processed by Interrupted Aging, *Mater. Sci. Eng. A*, 2014, **590**(1), p 97–100
6. G. Gu, L.Y. Ye, H.C. Jiang, D.X. Sun, P. Zhang, and X.M. Zhang, Effects of T9I6 Thermo-mechanical Process on Microstructure, Mechanical Properties and Ballistic Resistance of 2519A Aluminum Alloy, *Trans. Nonferr. Met. Soc. China*, 2014, **24**(7), p 2295–2300
7. D.X. Sun, X.M. Zhang, L.Y. Ye, G. Gu, H.C. Jiang, and G.X. Hui, Evolution of θ' Precipitate in Aluminum Alloy 2519A Impacted by Split Hopkinson Bar, *Mater. Sci. Eng. A*, 2015, **620**, p 241–245
8. C. Perrin and W.M. Rainforth, The Coarsening of θ Precipitates in an Al-4WT% Cu Alloy as a Result of Frictional Heating, *Scr. Mater.*, 1996, **34**(6), p 877–881
9. Z.G. Gao, X.M. Zhang, Y.S. Zhao, M.A. Chen, and H.J. Li, The Effect of Strain Rate on the Microstructure of 2519A Aluminum Alloy Plate Impacted at 573K, *J. Alloy. Compd.*, 2009, **481**(1–2), p 422–426
10. Z.G. Gao, X.M. Zhang, and M.A. Chen, Influence of Strain Rate on the Precipitate Microstructure in Impacted Aluminum Alloy, *Scr. Mater.*, 2008, **59**(9), p 983–986
11. W.H. Liu, Z.T. He, Y.Q. Chen, and S.W. Tang, Dynamic Mechanical Properties and Constitutive Equations of 2519A Aluminum Alloy, *Trans. Nonferr. Met. Soc. China*, 2014, **24**(7), p 2179–2186
12. A. Azimi, G.M. Owolabi, H. Fallahdoost, N. Kumar, and G. Warner, High Strain Rate Behavior of Ultrafine Grained AA2519 Processed via Multi Axial Cryogenic Forging, *Metals*, 2019, **9**, p 115
13. A. Azimi, G.M. Owolabi, H. Fallahdoost, N. Kumar, and G. Warner, Dynamic Failure Investigation in Ultrafine Grained AA2219: Mechanical and Microstructural Analysis, *Metals and Materials International*, 2019, p 1–12
14. A.T. Olasumboye, G.M. Owolabi, A.G. Odeshi, N. Yilmaz, and A. Zeytinci, Dynamic Behavior of AA2519-T8 Aluminum Alloy Under High Strain Rate Loading in Compression, *J. Dyn. Behav. Mater.*, 2018, **4**(1), p 1–11
15. G.M. Owolabi, D.T. Bolling, A.G. Odeshi, H.A. Whitworth, N. Yilmaz, and A. Zeytinci, The Effects of Specimen Geometry on the Plastic Deformation of AA 2219-T8 Aluminum Alloy Under Dynamic Impact Loading, *J. Mater. Eng. Perform.*, 2017, **26**(12), p 1–10
16. G.M. Owolabi, D.T. Bolling, A.A. Tiamiyu, R. Abu, A.G. Odeshi, and H.A. Whitworth, Shear Strain Localization in AA 2219-T8 Aluminum Alloy at High Strain Rates, *Mater. Sci. Eng. A*, 2016, **655**(2), p 212–220
17. D.X. Sun, X.M. Zhang, L.Y. Ye, X.H. Gui, H.C. Jiang, and G. Gu, Comparative Study of the Dynamic Mechanical Behavior of Al-

- minum Alloy 2519A and 7039, *Mater. Sci. Eng. A*, 2015, **640**, p 165–170
18. S.Y. Hu, M.I. Baskes, M. Stan, and L.Q. Chen, Atomistic Calculations of Interfacial Energies, Nucleus Shape and Size of θ' Precipitates in Al–Cu Alloys, *Acta Mater.*, 2006, **54**(18), p 4699–4707
 19. Y. Feng, Z.Z. Zhu, F.Q. Zu, S.S. Hu, and P. Yi, Strain Rate Effects on the Compressive Property and the Energy-absorbing Capacity of Aluminum Alloy Foams, *Mater. Charact.*, 2001, **47**(5), p 417–422
 20. R. Saha and R.K. Ray, Microstructural and Textural Changes in a Severely Cold Rolled Boron-Added Interstitial-free Steel, *Scr. Mater.*, 2007, **57**(9), p 841–844
 21. D.O. Ovono, I. Guillot, and D. Massinon, Determination of the Activation Energy in a Cast Aluminium Alloy by TEM and DSC, *J. Alloy. Compd.*, 2007, **432**(1), p 241–246
 22. H. Fara and R.W. Balluffi, Analysis of Diffusion in Media Undergoing Deformation, *J. Appl. Phys.*, 1958, **29**(7), p 1133–1134
 23. G.R. Love, Dislocation Pipe Diffusion, *Acta Metall.*, 1964, **12**(6), p 731–737
 24. E.W. Hart, On the Role of Dislocations in Bulk Diffusion, *Acta Metall.*, 1957, **5**(10), p 597–597
 25. A.W. Zhu, J. Chen, and E.A. Starke, Jr., Precipitation Strengthening of Stress-aged Al–xCu Alloys, *Acta Mater.*, 2000, **48**(9), p 2239–2246

Publisher's Note Springer Nature remains neutral with regard to jurisdictional claims in published maps and institutional affiliations.